Atmospheric Research 199 (2018) 82–92

Contents lists available at ScienceDirect

Atmospheric Research

journal homepage: www.elsevier.com/locate/atmosres

Numerical Study of Motion of Falling Conical Graupel

Chih-Che Chueh[a], Pao K. Wang[a,b,*], Tempei Hashino[c]

[a] Research Center for Environmental Changes, Academia Sinica, Taipei, Taiwan
[b] Department of Atmospheric and Oceanic Sciences, University of Wisconsin-Madison, WI 53706, USA
[c] Research Institute for Applied Mechanics, Kyushu University, Japan

ARTICLE INFO

Keywords:
Fall attitudes
Conical graupel particles
CFD
Low Reynolds numbers

ABSTRACT

In the present study, the attitudes of freely-falling conical graupel with a realistic range of densities are investigated numerically by solving the transient Navier-Stokes equations and the body dynamics equations representing the 6-degrees-of-freedom motion. This framework allows us to determine the position and orientation of the graupel in response to the hydrodynamic force of the flow fields. The results show more significant horizontal movements than those cases with a fixed bulk density of ice assumed in our previous study. This is because the real graupel particles possess the density less than the bulk density of ice, which, in turn, leads to a relatively small mass and a relatively small set of moments of inertia. We demonstrate that, with the six degrees of freedom considered together, when Reynolds number is small, a typical damped oscillation occurs, whereas when Reynolds number is high, amplifying oscillation may occur which leads to more complicated and unpredictable flying attitudes such as tumbling. The drag coefficients obtained in the present study agree with the previous studies and can be approximated by that of spheres of the same Reynolds numbers. We also show that conical graupel can perform significant horizontal translations which can be on the order of 1 km in 1 h.

1. Introduction

Graupel (or soft hails) are the precursor of hailstones and often conical in shape. In cloud physics, graupel is defines as an ice particle grown mainly by the riming process and with a size < 5 mm (Pruppacher and Klett, 1997). Further growth of graupel will lead to the formation of hailstones. The riming process refers to the collision of ice particles with supercooled water droplets that subsequently freeze on the ice surface (Pruppacher and Klett, 1997; Wang, 2013). Riming is a phase change process and hence is accompanied by the release of latent heat. Rapid riming of graupel can cause very fast latent heat release and influence the cloud development via rapid heating in the cloud. The riming rate depends on the collision efficiency (Wang, 1983) between the graupel and the supercooled droplets which, in turn, depends greatly on the fall attitude of the graupel. The fall of the graupel generates a flow field around it and that field controls whether or not the droplet can collide with the graupel.

Aside from forming hailstones that can cause severe damage to crops and properties, collision of graupel and ice crystals is thought to be a major electrification mechanism of thunderclouds (Takahashi, 1978 and Williams and Zhang, 1996). How fast electric charges can accumulate in the cloud depends greatly on the collision efficiency which again depends mainly on the flow field of the falling graupel.

The flow field of a falling ice particle is affected greatly by its shape and size. A small ice particle falls smoothly and the flow field is laminar. As the particle increases in size, the flow field becomes increasingly turbulent. Highly nonspherical ice particles such as hexagonal ice columns, hexagonal ice plates and conical graupel can perform wide translational and rotational, even tumbling movements (e.g., Field et al., 1997; Hashino et al., 2016; Vincent et al., 2016; Chueh et al., 2017). Chueh et al. (2017) reported some preliminary numerical results of the fall of conical graupel in order to understand their basic fall attitudes. They obtained results that are qualitatively consistent with experimental results of the vertical wind tunnel study by Pflaum et al. (1978; 1979; 1980). However, the graupel density used in Chueh et al. (2017) is assumed to be constant (i.e., that of solid ice) which is unrealistic. It is known that graupel density vary greatly with size and hence the mass and therefore the fall velocity of the graupel (Pruppacher and Klett, 1997). All these will ultimately impact the fall attitude of the graupel.

The aim of the present paper is to allow the graupel density to vary according to the size so that the results of the present simulations having the realistic density values and thus the more realistic mass and moment of inertia of the graupel can reflect the physics of the freely falling conical graupel particles. We will also perform more thorough analyses of the flow fields in order to better understand the fall

* Corresponding author at: Department of Atmospheric and Oceanic Sciences, University of Wisconsin-Madison, 1225 W. Dayton St., Madison, WI 53706, USA.
E-mail address: pwang1@wisc.edu (P.K. Wang).

http://dx.doi.org/10.1016/j.atmosres.2017.09.008
Received 3 June 2017; Received in revised form 20 August 2017; Accepted 12 September 2017
Available online 14 September 2017
0169-8095/

behavior, especial those related to tumbling which is a very important fall mode of graupel especially when they become larger.

This paper is organized as follows. In Section 2, the mathematical and physical background of the governing equations and the mathematical expressions used to generate the conical graupel shape are presented. This is followed by the results and their discussions of the motions of these particles. Finally, the conclusions and outlook will be given in the final section.

2. Physics and mathematics of the flow field calculations

Following the previous study by Chueh et al. (2017), we use the same equation to depict the x-z-cross-section of the graupel shape first proposed by Wang (1982). This equation is:

$$x = \pm a\sqrt{1-\left(\frac{z}{c}\right)^2}\cos^{-1}\left(\frac{z}{\lambda c}\right), \tag{1}$$

where x and z are the horizontal and vertical coordinates whereas a and c are used to control the horizontal and vertical semi-axis lengths, respectively. The parameter λ, whose value varies between 1 and ∞, serves to control the sharpness of the apex of the conical graupel. For more details about this expression and the shape it generates, see Wang (1982).

Eq. (1) generates only the xz-cross-section of the graupel. To obtain a 3D conical body, we revolve this cross-section about the z-axis which yields the following 3D mathematical expression:

$$\frac{x^2}{(a\ \cos^{-1}(z/\lambda c)^2)}+\frac{y^2}{(a\ \cos^{-1}(z/\lambda c)^2)}+\frac{z^2}{c^2}=1, \tag{2}$$

which is a special case of the conical bodies with elliptical cross-sections descried by Wang (1999).

Using Eq. (2) and assuming various combinations of a, c and λ, we can generate conical graupel of different sizes and shapes (Wang, 1982). The parametrical combinations we use in the present study are the same as that in Chueh et al. (2017).

For the fall of hydrometeors in clouds, the scale is small enough so that the compressibility of air plays no important role (Pruppacher and Klett, 1997; Wang, 2013). Thus we only need to consider incompressible flow for the present study. For isothermal, incompressible flow of a Newtonian air fluid, the mass and momentum transport are described as follows:

$$\nabla\cdot\mathbf{u} = 0, \tag{3}$$

$$\frac{\partial\mathbf{u}}{\partial t}+(\mathbf{u}\cdot\nabla)\mathbf{u}=-\frac{\nabla p}{\rho_a}+\nu\nabla^2\mathbf{u}+\mathbf{g}, \tag{4}$$

where $\mathbf{u}$ stands for the air velocity vector containing three components representing u_1, u_2, and u_3 in x, y, z direction, respectively, p the pressure, ρ_a the air density, ν the kinematic viscosity of air, and $\mathbf{g}$ the gravity. The boundary conditions are the same as in Hashino et al. (2016):

$$u_i = 0\ \ (i = 1,2,3)\,\text{at graupel particle surface}, \tag{5}$$

$$u_3 = u_\infty = \text{constant at the inlet of the outmost boundary from graupel}, \tag{6}$$

$$\frac{\partial u_3}{\partial z} = 0\ \text{at the outlet of the outmost boundary from graupel}, \tag{7}$$

$$u_1 = u_2 = 0,\ \frac{\partial u_i}{\partial x}=\frac{\partial u_i}{\partial y}=0\ \ (i = 1,2,3)\,\text{at the lateral side of outmost boundary from graupel}, \tag{8}$$

The physical meaning of these boundary conditions can be found in Chueh et al. (2017). The boundary condition (5) is the nonslip condition for the dynamic mesh considered here.

In this study, conical graupel particles with diameters of 0.5, 1, 2, 3, 4, 5 mm are investigated. As mentioned before, graupel becomes hailstones when they are larger than 5 mm. The present study assumes that the atmospheric environment is that pressure is 800 hPa and temperature is −8 °C. In such an environment, the temperature is in the warm range (from 248 to 278 K) where graupel particles are typically found (Pruppacher and Klett, 1997). The atmospheric environment is the same as those used previously in Wang and Kubicek (2013), Hashino et al. (2014, 2016), and Chueh et al. (2017). The graupel's far stream velocity u_∞ values were set to the terminal fall velocities estimated based on the empirical velocity-mass relationship for conical graupel by Locatelli and Hobbs (1974). The values are calculated based on a mathematical equation in their Table 1.

The motion of the graupel in the present study is not pre-determined; its position and orientation at each time step is determined by the hydrodynamic forces calculated at the previous time step (see Snyder et al., 2003). To achieve this, we employed the six degrees of freedom (6 DoFs) solver in the computational fluid dynamics package ANSYS Fluent (http://www.ansys.com/Products/Fluids/ANSYS-Fluent) which uses forces and moments acting on the graupel in order to compute the translational and angular motion of the center of gravity of an object. All the details about how we calculate the moment of inertia of the conical graupel and how it works inside ANSYS Fluent can be found in Chueh et al. (2017). The numerical schemes we use here are also the same as that described in Hashino et al. (2016) and Chueh et al. (2017).

In the present study, the method of creating a mesh with the curved shape of the conical graupel is the same as the one used by Kubicek and Wang (2012), Wang and Kubicek (2013), and Chueh et al. (2017), and is briefly outlined as follows. First we calculate the graupel surface coordinates by using Eq. (1) for the half of the x-z-cross section and then revolve the half-curved cross section 360° about z axis to yield the 3D conical shape. This is done by using ANSYS DesignModeler.

The dynamic conical graupel simulation (Chueh et al., 2017) requires changing the mesh around the conical graupel at every time step as the graupel falls. However, re-meshing the computational domain at every time step can significantly slow down the computation, making the simulation inefficient and difficult to perform. In order to increase the computational efficiency, we do not re-mesh the whole computational domain at every time step, but rather re-generate the mesh for only few sub-domains close to the graupel surface, which was used in Cheng et al. (2015), Hashino et al. (2016) and Chueh et al. (2017) for the freely falling hexagonal plates, ice columns, and conical graupel, respectively. The mesh used here is adapted to suit the need of the changing graupel orientation and environmental flow field, ensuring that we can preserve adequate accuracy of the computed flow fields and at the same time enhance the computational efficiency, as described for the benefits of the use of the adaptive grids (see, e.g., Chueh et al., 2010, 2013).

We use Tait-Bryan angles (Landau and Lifshitz, 1969; Goldstein, 1980) associated with the orientations of the graupel to quantitatively describe their orientation behavior as shown in Fig. 1a. The angles (i.e., θ_x, θ_y, and θ_z) are defined as the rotation about the global fixed x, y, and z axes passing through the center of gravity of the graupel, respectively.

2.1. Initial perturbation

Like our previous three studies (Cheng et al., 2015; Hashino et al., 2016; and Chueh et al., 2017), we produce an initial perturbation in the flow field around the graupel to quickly initiate the unsteady motion of the falling graupel. This is done by using an initial inclination angle of 20° counterclockwise around the y'' axis, as shown in Fig. 1(b). The small initial inclination angle is intended to produce a correspondingly small perturbation, which induces rotating oscillations of the falling graupel. The definition of the positive sign of the initial inclination of the conical graupel (i.e. $\theta_y = 20°$) can be found in Fig. 1(b). Then, a steady flow solution is obtained for the inclined state of the graupel

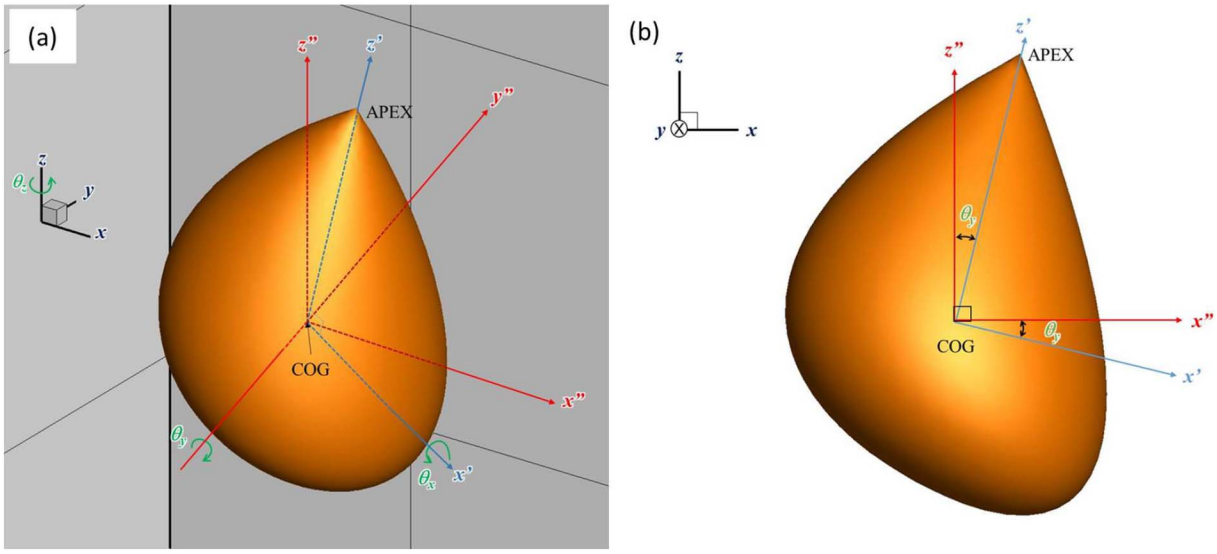

Fig. 1. Definition of the coordinates and Tait-Bryan orientation angles in (a) 3D view and (b) on the *xy*-plane used in the present study. The global coordinates are represented in black by the *x*, *y* and *z*. The x'', y'' and z'' axes passing through the center of gravity (COG) of the graupel particle in red are parallel to the global axes *x*, *y* and *z* respectively. The z' axis perpendicular to the x' axis in blue is a line linking both COG and the apex of the graupel. The change in orientation from x'' to x' conforms to the change from z'' to z' so that x' and z' remain perpendicular to each other in the 3D space. θ_x, θ_y and θ_z are defined in green as the rotation angles around x', y'' and *z* axes respectively. Note that the representation of the dotted line segments for parts of the axes means that they are situated inside the graupel. (For interpretation of the references to colour in this figure legend, the reader is referred to the web version of this article.)

with a constant u_∞ and serves as the initial condition of the freely falling conical graupel simulation.

In the present study, we investigate the fall attitudes of the same set of conical graupel particle sizes and shapes as specified by Chueh et al. (2017). The shape parameters *a*, *c* and λ of the graupel as well as their corresponding far field velocities, and the terminal velocities of the graupel are given in Table 1. The negative V_t values indicate that graupel are falling relative to the computational domain which is called the computational "wind tunnel". We divide the wind tunnel into a few different computational zones similar to that used by Hashino et al. (2016) and Chueh et al. (2017). The mesh of one of the computational zones, the one closest to the outer boundary of the entire domain, is always kept unchanged throughout every of the simulations performed here, whereas the meshes of the rest zones either change or move with the graupel at every time step, as the falling graupel changes its orientation and position with time.

Because the motion of the graupel is unsteady and its velocity can change substantially with changing fall attitude, there is a need to define two different Reynolds numbers so as to describe the instantaneous motion in better clarity. We use the following two definitions of Reynolds number. The regular Reynolds number is defined as

$$N_{\mathrm{Re}} = \frac{d u_\infty}{\nu}, \tag{9}$$

where *d* is the diameter of the graupel representing its maximum width in *x* and *y* directions, and u_∞ is defined in Eq. (6). The quasi-steady state Reynolds number is defined as.

$$N_{\mathrm{Re}\,q} = \frac{d(u_\infty - V_t)}{\nu}, \tag{10}$$

where the relative terminal fall velocity values of V_t are obtained from the simulations that already reach their individual steady-state fall velocity values (Vel_z). The quasi-steady state Reynolds numbers are considered as the actual ones that are calculated and listed in Table 1.

2.2. Graupel density determination

Direct measurements of graupel density are rare and the results have considerable scatter mainly because many graupel are not of standard conical shape and their grain structures may differ from each other. The two sources we found that are useful to the present study are Locatelli and Hobbs (1974) and Heymsfield and Kajikawa (1987), both are based on observations. We decided to develop a scheme based on the measurements of Locatelli and Hobbs (1974). We determined the density of a graupel by dividing the graupel mass observed by Locatelli and Hobbs (1974) by the volume calculated from Eq. (2). The results are shown in Table 2. These values are much smaller than the constant density 0.91668 g/cm^3 of solid ice used in our previous study (Chueh et al., 2017) but are more realistic, as most real graupel particles are mixtures of solid and porous ice particles, and the density should be smaller than that of solid ice.

As a comparison, we also calculated graupel density based on the mass-diameter relation given by Heymsfield and Kajikawa (1987, their Table 2) for conical graupel for $T < -0.5$ °C and yielded the following values: 0.210 g cm^{-3} (d = 0.5 mm), 0.193 (1.0), 0.177 (2.0), 0.169

Table 1
Dimension, far field and terminal velocity, and terminal velocities of the graupel investigated in this study. See the text for detailed definitions.

d (mm)	u_∞ (m s^{-1})	V_t (m s^{-1})	N_{Re} *(Normal)*	N_{Req} *(quasi-steady)*
0.5	0.5	− 0.17	15.6	21
1	0.97	− 0.1754	60.7	71.6
2	1.67	− 0.27	209	243
3	2.06	− 0.3	387	443
4	2.32	− 0.34	580	665
5	2.55	− 0.48	797	948

Table 2
Graupel ice density values of the conical graupel particles considered herein.

d (mm)	Graupel ice density (g cm^{-3})
0.5	0.245
1	0.186
2	0.141
3	0.12
4	0.107
5	0.0977

(3.0), 0.163 (4.0), and 0.159 (5.0). Comparing these values with that in Table 2, we see that while there are differences, especially in the large end, they are in the same order of magnitude. In addition, both show decreasing density with increasing size. Given that there are many other factors such as asymmetric shape, irregularities on the surface, and internal inhomogeneity, we feel that values listed in Table 2 are acceptable.

More recently, Enzmann et al. (2011) developed a technique to quantify graupel porosity. They developed a 3-D imaging system using synchrotron-based micro-tomography to reconstruct graupel microstructures. Hopefully this technique can be applied by researchers to determine more precisely graupel density in the future.

3. Results and discussions

3.1. Fall attitudes

The fall attitude of conical graupel had been studied previously. List and Schemenauer (1971) used artificial conical graupel models to drop into glycerin-water mixtures and salt solutions to study how they fall. Kajikawa (1977) made direct observations of the fall attitudes of natural graupel. Their results differ in details mainly owing to the differences in particle shapes and surface roughness as noted by Kajikawa (1977). However, the reported general behaviors are similar. The conical graupel particles < 1 mm and $N_{Re} < 100$ fell in stable, base down orientation. When the particle diameters were ~ 3.5 mm, oscillation began at $N_{Re} \sim 100$ and the onset of tumbling at $N_{Re} \sim 700$. In terms of the fall attitudes of the freely falling conical graupel, these are more or less consistent with the present results we will show subsequently.

As mentioned previously, Chueh et al. (2017) made the first theoretical study of the free fall behavior of conical graupel. They described the fall attitudes of conical graupel covering the same shape and size ranges as the present study. While the fall attitudes they reported were qualitatively consistent with that observed in the laboratory, the graupel density was held constant at 0.91668 g cm^{-3} and thus not as realistic as it should be. In the present study, we investigate the fall behavior of a group of conical graupel of the same sizes and shapes but with varying density as described in the previous section, hence the results are more realistic. In the following, we will summarize the new results and also give a more through discussion of the fall attitudes and other hydrodynamic properties of these conical graupel.

The present results show that the fall attitudes of this group of graupel can be classified into 3 categories: (1) damped oscillation ($d = 0.5$ mm); (2) persistent oscillation but no tumbling ($d = 1$ and 2 mm); (3) persistent tumbling ($d \geq 3$ mm). These will be described in more detail in the following.

3.1.1. Damped oscillation ($d = 0.5$ mm)

Fig. 2 shows, from left to right, the pressure and z-speed distributions in the central x-z plane, and the streamtrace pattern of the steady state flow field of a conical graupel of $d = 0.5$ mm falling at terminal velocity. Such flow fields have been described in detail by Kubicek and Wang (2012) and Wang and Kubicek (2013).

As mentioned before, we produced a small perturbation in the flow field by tilting the graupel vertical axis 20°. The viscous effect of air soon diminishes this small perturbation and the graupel returns to upright orientation and falls vertically.

Fig. 3 shows the time behavior of a few key kinematic variables of the fall motion of a graupel of $d = 0.5$ mm. The damped oscillation phenomenon, e.g., cg_x in (a), Vel_x in (c), θ_y in (e) and T_y in (f), is obvious. They all demonstrate that the perturbation caused oscillation is damped by the viscous effect of air. The rest of variables, such as cg_y, cg_z, Vel_y and Vel_z exhibit little or non-oscillatory behavior, as they are expected to be. In addition to oscillation, Fig. 3(a) also shows that the x-y position of the graupel has moved away from the origin, especially in the x-direction. The y-position changed little.

Fig. 4 shows the plot of torque acting on the graupel as a function of the tilt angle. The starting tilt angle is 20° (the blue circle on the extreme right). We see that the torque increases initially until the tilt reaches the negative maximum as the graupel oscillates, then decreases again as the graupel swings back. Eventually the torque settles in the purple and red region in Fig. 4 as the oscillation is dwindling. We see that the final stage of the torque variation with angle is consistent with that predicted by the theory of Cox (1965) and that of potential flow for small spheroids (see Hashino et al., 2016, for more details).

3.1.2. Persistent oscillation but no tumbling ($d = 1$ and 2 mm)

For larger conical graupel of $d = 1$ and 2 mm, the fall behavior turns to that of persistent and periodic oscillation but no tumbling. We shall use the case of $d = 1$ mm to illustrate this fall attitude.

Fig. 5 shows, from left to right, the pressure, z-velocity and streamtrace fields, respectively, of a randomly chosen snapshot of the unsteady flow field around the falling graupel of $d = 1$ mm. Unlike the $d = 0.5$ mm case, this graupel now performs persistent periodic oscillatory motions in the horizontal plane during its fall. The magnitudes of the pressure deviations and the size of the recirculation bubble are larger than the $d = 0.5$ mm case, as they should be.

Note that the present unsteady flow case is different from the cases reported in Wang and Kubicek (2013) where the graupel is held at a fixed orientation, hence no flow field feedback on the motion of the graupel is considered there. In the present case, the graupel is allowed to adjust its position and orientation according to the hydrodynamic force and torque acting on it, and therefore one should not expect the flow field in the present case be the same as the graupel in Wang and Kubicek (2013) even if the size, shape, and 3-D orientation of the two graupel are completely the same at that moment.

Fig. 6 a group of plots of kinematic variables as a function of time. Now the persistent periodic motion is most obvious in cg_x, Vel_x, θ_y and T_y. At the same time, we also see that there is also a corresponding periodic motion in y-direction as demonstrated by the curves of cg_y, Vel_y, θ_x and T_x, although the amplitudes are smaller. The oscillation in the y-direction exhibits an amplifying tendency. The same thing happens in the corresponding kinematic variables in the z-direction but the amplitudes are even smaller. Obviously the zigzag motion in the x-direction must have influenced the flow field such that the graupel's motions in the y- and z-direction also become periodic.

We did not investigate the possibility that the amplifying oscillation in the x- and z-direction would eventually lead to tumbling, as this requires to run the calculation for much longer time. We will investigate this possibility in the future.

From Fig. 6(a), it also appears that cg_y is increasingly negative, i.e., the y-position of the graupel deviates more and more from its original place while cg_x remains oscillatory at about the same x-coordinate. Overall, this indicates that, as time goes on, the graupel will translate horizontally further and further away from its original position. This fact may be of some importance to cloud physics and we will expand more on this point later.

Fig. 7 shows the calculated torque as a function of tilt angle. We see that the relation is now quite different from that predicted by Cox (1965) and the potential flow theory. This is not surprising as Cox's theory only applies to very low Reynolds numbers while the potential flow theory ignores the viscous effect totally. Both are not true for the present case.

3.1.3. Persistent tumbling ($d \geq 3$ mm)

For graupel of $d \geq 3$ mm, the fall attitude changes to persistent tumbling. We will use the $d = 5$ mm graupel to illustrate such fall attitude. Fig. 8 shows a random frame of the pressure, z-velocity and streamtrace fields in the central xz-plane of the flow field around a falling conical graupel of $d = 5$ mm. Again, while the pattern may look similar to that reported by Wang and Kubicek (2013), the reader is

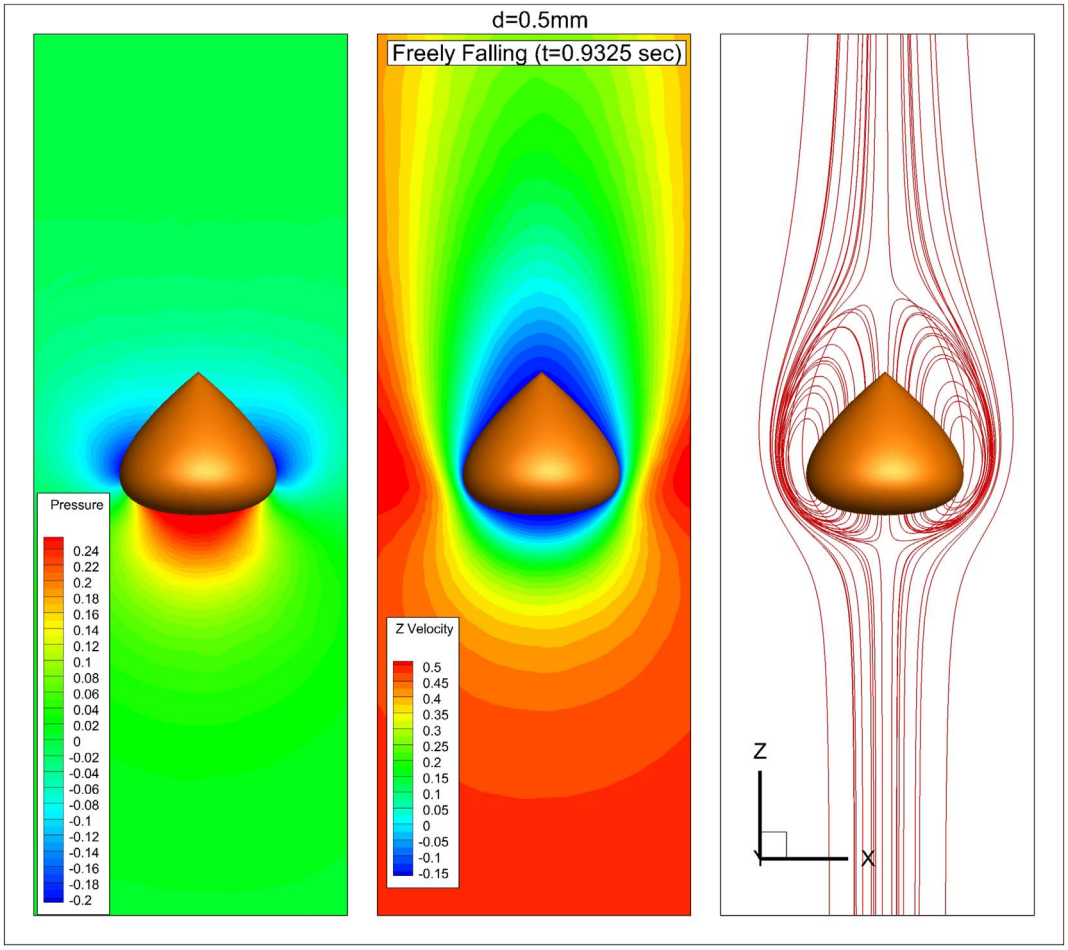

Fig. 2. A snapshot of the flow field in the central xz-plane around a falling conical graupel of $d = 0.5$ mm: (left) pressure distribution, (center) z-velocity distribution, and (right) streamtraces.

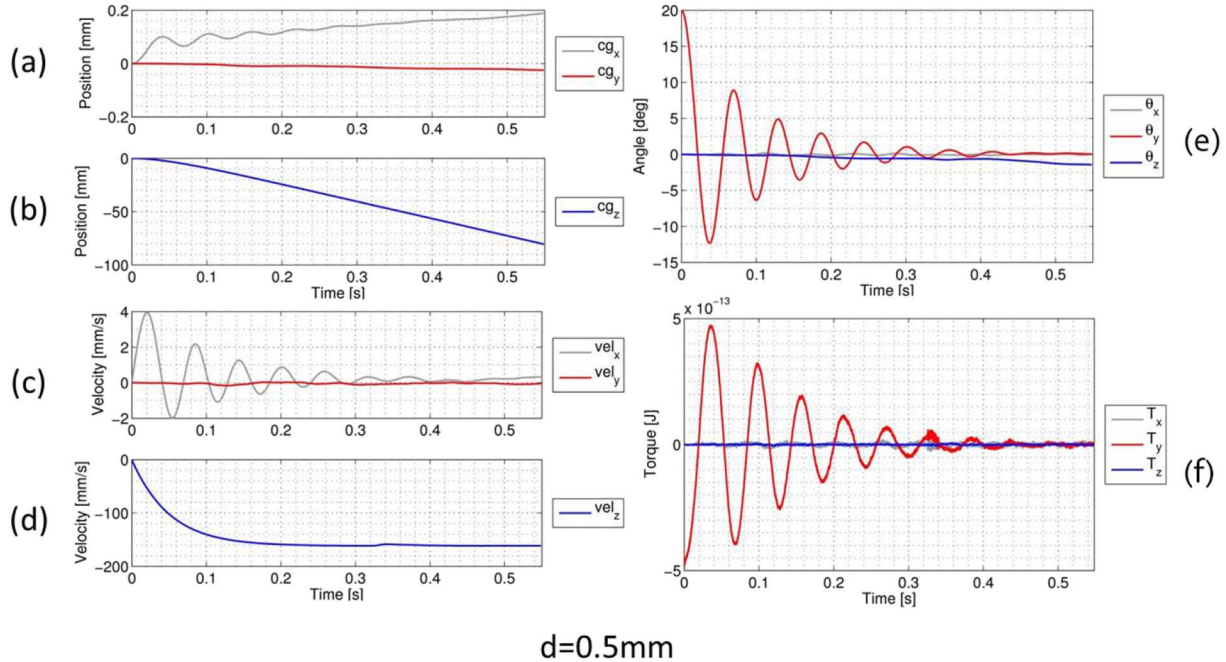

Fig. 3. Time variation of a few key kinematic variables for a falling conical graupel of $d = 0.5$ mm: (a) the x and y positions of COG, cg_x and cg_y, respectively, (b) the z position of COG, cg_z, (c) x and y-components of the graupel velocity vel_x and vel_y, (d) vel_z, (e) Tait-Bryan angles θ_x, θ_y and θ_z, (f) torques T_x, T_y, T_z.

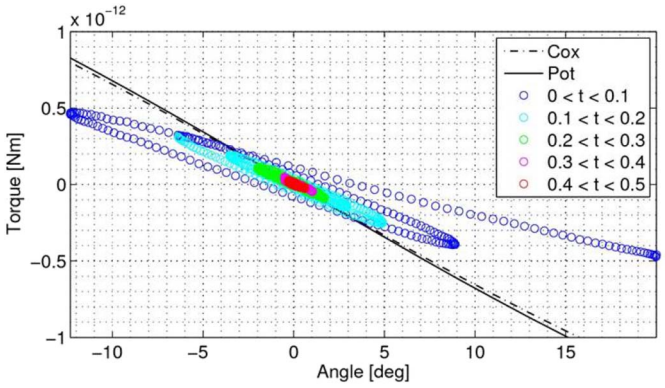

Fig. 4. The torque on the graupel as a function of θ_y. Different colors represent different time periods (in seconds) as indicated in the legend box. (For interpretation of the references to colour in this figure legend, the reader is referred to the web version of this article.)

reminded that the graupel in the present study is falling freely and the flow field's feedback on the graupel motion is in action, hence the flow fields may differ significantly even if the size, shape and orientation of the two graupel are completely the same at an instant.

Fig. 9 shows the time variation of kinematic variables of the 5 mm graupel. We now see that the fall attitude of this graupel differs significantly from the previous two categories. Fig. 9(a) shows that both cg_x and cg_y move away from the origin more and more as time goes on, implying that the graupel translates a significant distance horizontally. This sideway translation is far greater than that in the 1 mm case.

The tumbling motion triggers complex motion modes. Fig. 9(c) shows that Vel_x and Vel_y change significantly with time. The changes for larger particles are greater than that for smaller particles (note that the scales in different charts are different), for example, the graupel of $d = 5$ mm reaches maximum velocity of $\sim 0.4\ \mathrm{m\ s^{-1}}$ in x direction and $\sim 0.25\ \mathrm{m\ s^{-1}}$ in y direction, while it is $< 0.001\ \mathrm{m\ s^{-1}}$ for 0.5 mm and $< 0.01\ \mathrm{m\ s^{-1}}$ for 1 mm graupel in both directions. The larger changes for larger graupel is apparently associated with the tumbling motion. We see that the variation of Vel_x lags that of Vel_y, implying that the change in the latter induces the response of the former. There is also a more subtle response in Vel_z (Fig. 9(d)) which appears to stabilize after $t \sim 1.3$ s.

Fig. 9(e) shows the time variation of the three Tait-Bryan angles. It can be seen that the while θ_y is oscillatory throughout the simulation, both θ_x and θ_z go off the scale after $t \sim 0.4$ s. The latter indicates that the graupel becomes unstable and begins to tumble at this time.

To see clearer this behavior, we replot the time variation of θ_x and θ_y using different scales as shown in Fig. 10. Here we see that θ_x curve starts to go upward with values $> 360^\circ$ after $t \sim 0.4$ s, indicating that it tumbles over and over many cycles until $t \sim 1.3$ s when it begins to tumble in opposite direction.

Fig. 11 shows the change of torque with time of the falling 5 mm graupel. The torque behavior is much more complex than the two previous cases. Before tumbling occurs, the torque behaves more or less like that of the 1 mm graupel (blue circles) shown in Fig. 7, i.e., it already deviates significantly from the predictions by Cox (1965) and potential flow theories. As time goes on, however, the difference become greater (cyan, green and purple circles) and the nonlinear nature of the relation (the "S" shape of the curve) between the torque and

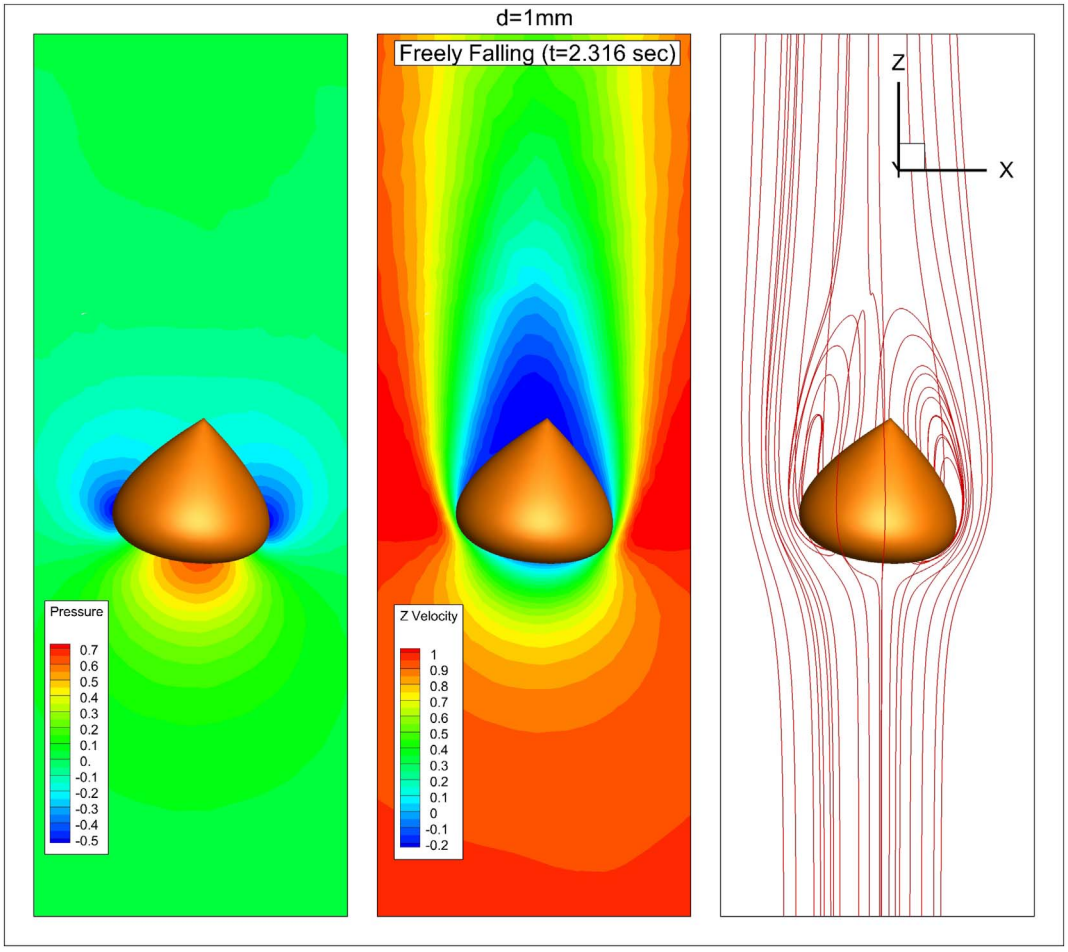

Fig. 5. Same as Fig. 2 except for $d = 1$ mm.

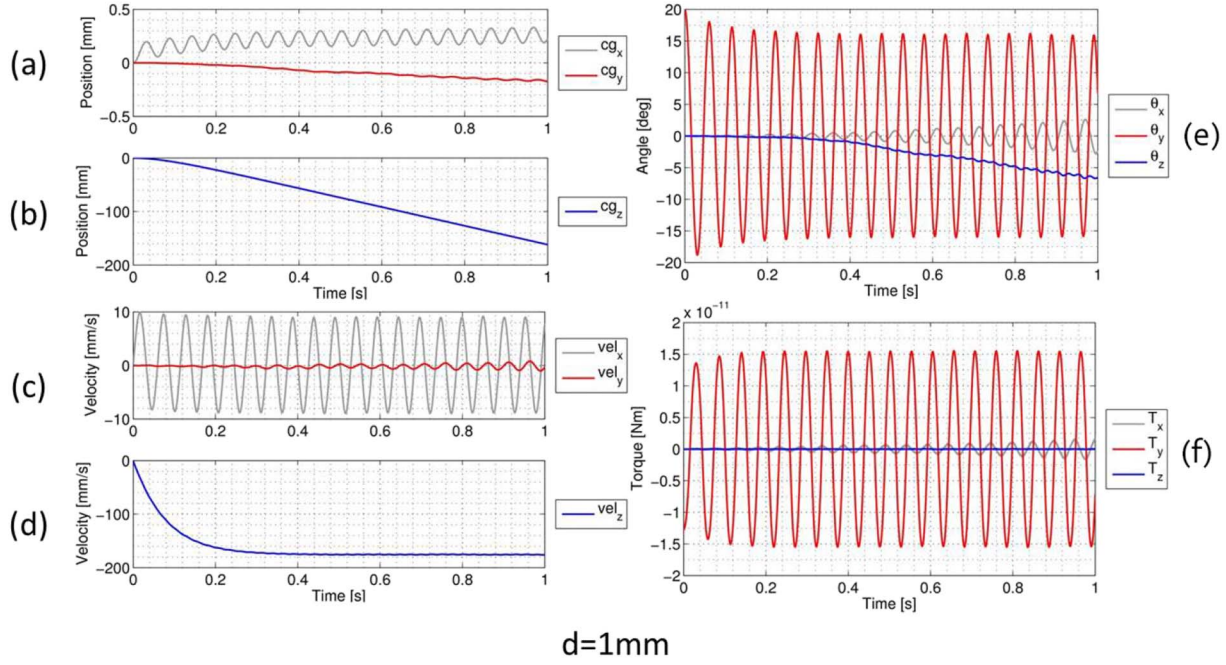

Fig. 6. Same as Fig. 3 except for $d = 1$ mm.

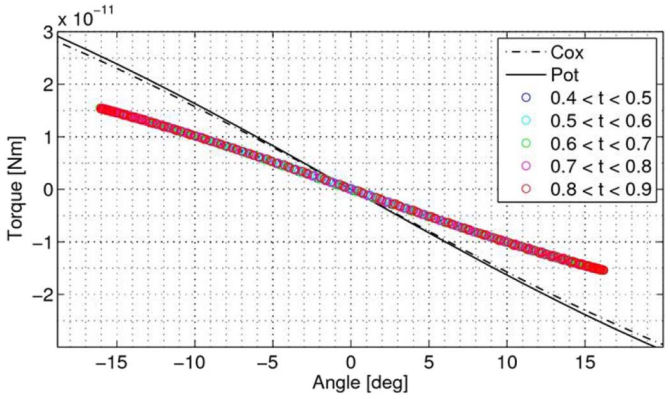

Fig. 7. Same as Fig. 4 except for $d = 1$ mm. (For interpretation of the references to colour in this figure, the reader is referred to the web version of this article.)

angle becomes more and more pronounced. Eventually tumbling occurs after $t \sim 0.4$ s (red circles) and the torque stops to be a single-valued but turns into a multivalued function of the tilt angle.

Tumbling of graupel was reported in the wind tunnel experimental studies of graupel by Pflaum et al. (1978). Since graupel is the precursor of hailstones and most of hailstones are roughly spheroidal (and thus lack the sharp apex like the conical graupel), we theorize that this may be the result of tumbling starting from the graupel when the latter become large enough.

In the above we have reported the kinematics of the tumbling. To understand the tumbling dynamics of conical graupel, we will need to make more careful analysis of the flow fields. We plan to perform this task and report the results in the near future.

Note that all the results reported above in Eqs. (1), (2) and (3) are based on the initial tilt $\theta_y = 20^\circ$ which is a very modest tilt. What if the initial tilt angle is larger than 20°? We have not yet made calculations on such cases but we feel it is likely to behave more or less the same, or perhaps tumbling will occur to graupel smaller than 3 mm. This will be left for future studies.

3.2. Horizontal displacement

The horizontal displacement of hydrometeors due to their fall attitude is a topic that is rarely treated in conventional cloud microphysics. It is usually assumed that an ice crystal falls vertically and collide with supercooled cloud drops when it is undergoing riming growth, even though it is widely known ice crystals and snowflakes may perform significant zigzag motions especially those of larger sizes. Such substantial horizontal movements may impact both cloud physics and cloud dynamics, for example, how large they will grow after a certain time period and where they can distribute in the cloud, and hence deserve more careful considerations.

It is seen in the above discussions that conical graupel may perform substantial horizontal movements during the fall. Fig. 12 shows the trajectory of the 5 mm graupel as it falls from its original position (0, 0, 0) during $t = 0$ to $t = 1.68$ s. Fig. 12(a) shows that the trajectory is a complicated spirally curve that leads to a horizontal position that is about 0.35 m away from the origin. Fig. 12(b) shows that the graupel orientation and horizontal position keeps changing as it falls. The simulated fall attitudes include all motion modes reported by Pflaum et al. (1978) who performed vertical wind tunnel study of graupel hydrodynamics. These motions include rotation, pendulum swing, sailing, and tumbling. Thus our study shows that the complicated motions of highly nonspherical ice hydrometeors such as conical graupel can be successfully simulated by computational fluid dynamics techniques. All these motion modes may impact the horizontal translation of graupel.

The average horizontal speed V_H of the graupel after it reached a quasi-steady fall attitude is shown in Fig. 13. In general, larger graupel tend to have larger horizontal speeds than smaller ones, although the 4 mm graupel has slightly higher V_H than the 5 mm graupel but the difference is small. Given a long time, the graupel may travel far from the origin as they fall. We see, for example, from Fig. 13(a) that V_H is about 0.31 m s^{-1} for $d = 5$ mm. Thus, in an hour the 5 mm graupel could potentially move a horizontal distance of ~1 km if it moves in the same direction away from the origin during this time period. Note this distance is translated purely due to the fall attitude of the graupel alone and has nothing to do with the in-cloud wind speed. This implies that the distribution of ice hydrometeors such as conical graupel in clouds can be much wider than predicted by cloud microphysical models that

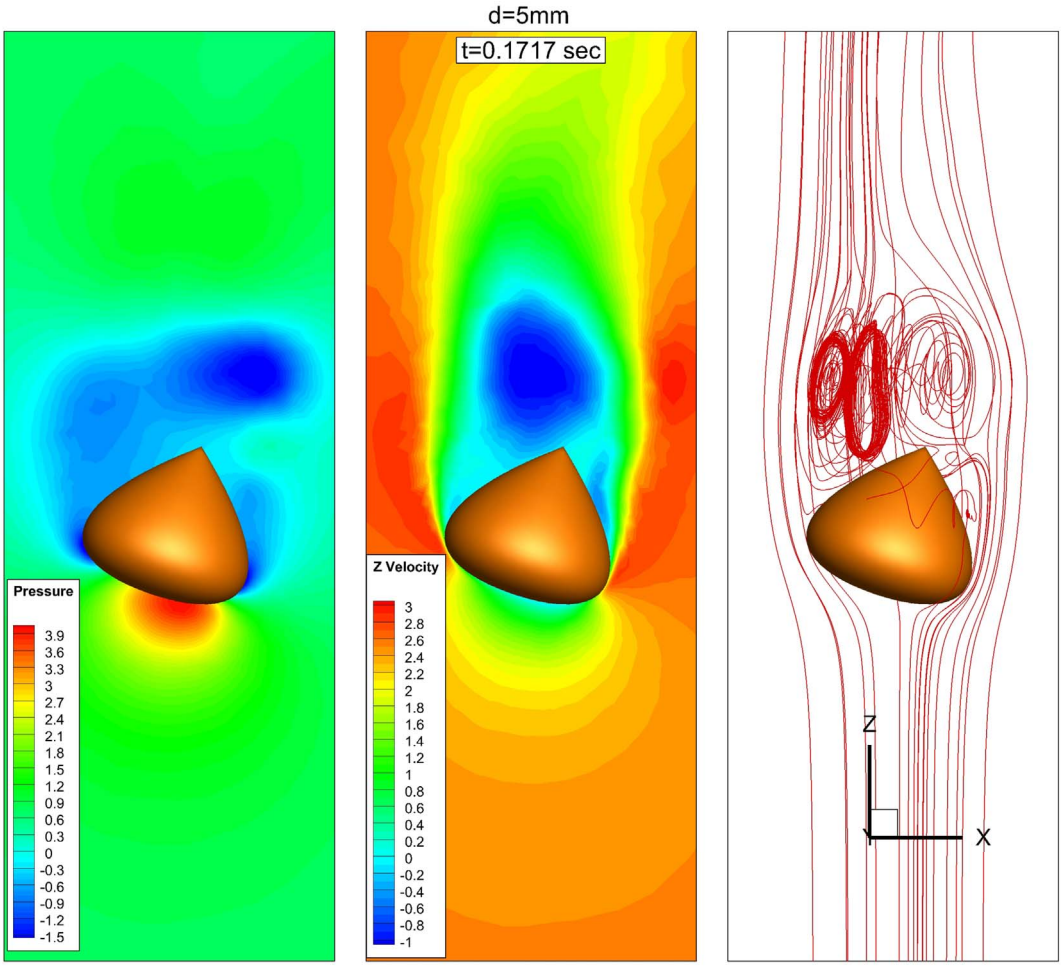

Fig. 8. Same as Fig. 2 except for d = 5 mm.

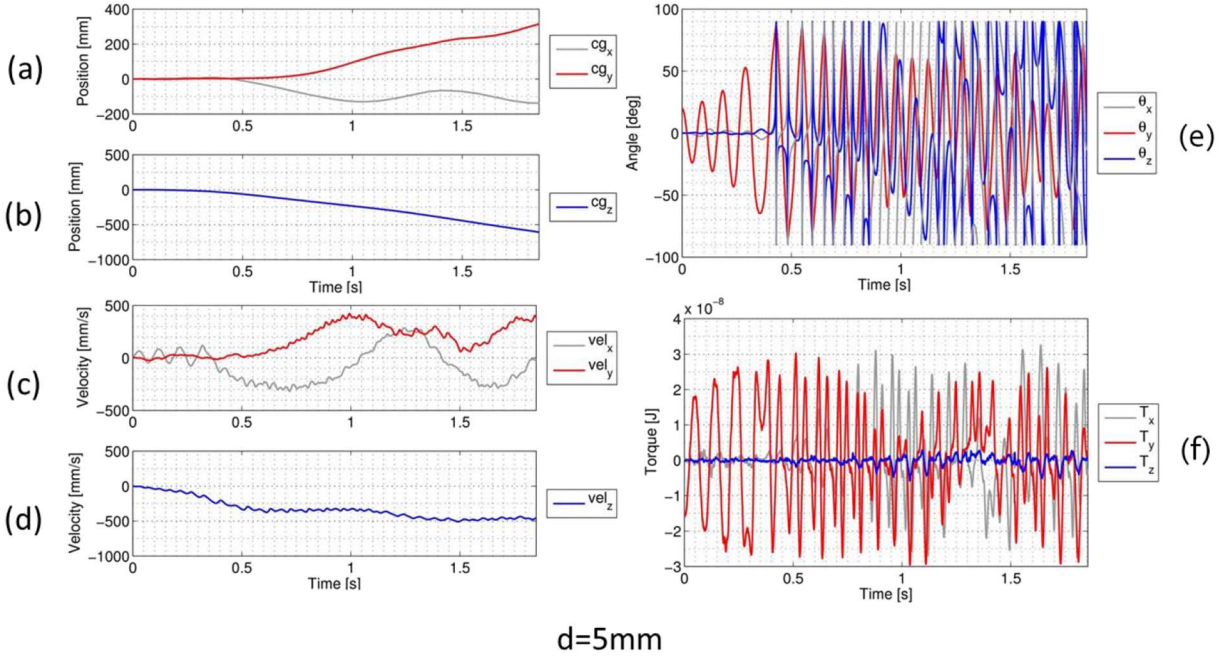

Fig. 9. Same as Fig. 3 except for d = 5 mm.

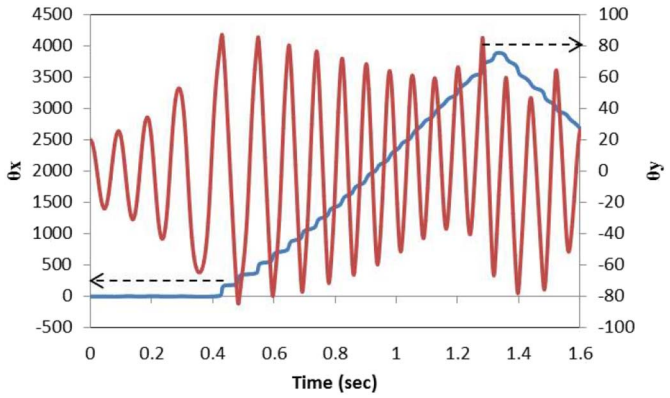

Fig. 10. θ_x and θ_y as a function of time for $d = 5$ mm.

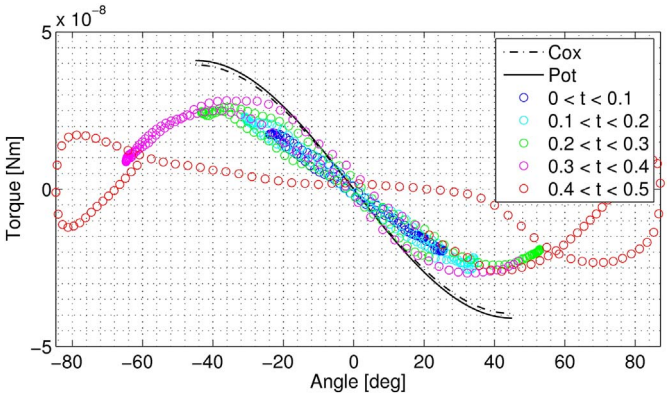

Fig. 11. Same as Fig. 4 except for $d = 5$ mm.

consider only vertical fall attitudes.

Fig. 13(b) shows the plot for V_H as a function of Reynolds number N_{Re}. We use linear fit for the data points in Fig. 13(a) and (b) as:

$$V_H = -0.06854 + 0.08126d \tag{11}$$

and

$$V_H = -0.01472 + 0.0003916N_{\mathrm{Re}} \tag{12}$$

Although a more sophisticated 3rd-order polynomial can fit the points better, it is felt unnecessary as there is no theoretical justification of such high-order fit.

3.3. Drag coefficients

The drag coefficients of the falling graupel after they reach steady state terminal fall velocity are calculated according to

$$C_D = \frac{2F_D}{\rho_a(u_\infty - V_t)^2 A_G}, \tag{13}$$

where F_D is the frag force acting on the graupel and A_G is the cross-sectional area of the graupel defined as a constant, $\pi(d/2)^2$. We used $(u_\infty - V_t)$ to obtain the quasi-steady Reynolds number as defined in Eq. (10). This is also consistent with that in Hashino et al. (2016).

Fig. 14 shows the comparison of the drag coefficients calculated in the present study with that of Wang and Kubicek (2013), sphere, Heymsfield and Kajikawa (1987) and Böhm (1992). We see that the present results are in general lower than that obtained by Wang and Kubicek (2013). This is likely due to the assumption on Wang and Kubicek (2013) that the graupel fall with fixed orientation whereas the present study allows the graupel to adjust the orientation in response to the instantaneous hydrodynamic force which tends to decrease the fluid resistance. Consequently the drag and hence the drag coefficients are generally lower in the present study.

In this regard, it is interesting to observe that the presently calculated drag coefficients are close to that of a sphere. This can be interpreted in the following manner. The reason why conical graupel drag deviates from that of a sphere is of course mainly due to its

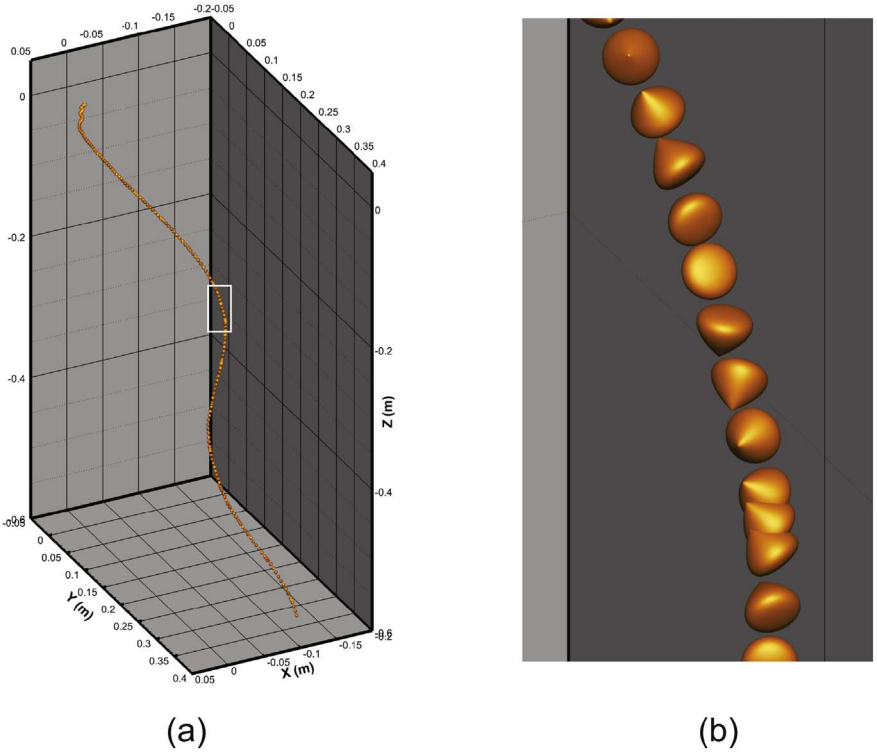

Fig. 12. Trajectory of the $d = 5$ mm graupel from $t = 0$ to $t = 1.68$ s. (a) Trajectory. (b) Enlarged view corresponding to the section indicated by the white box in (a) showing the fall orientations.

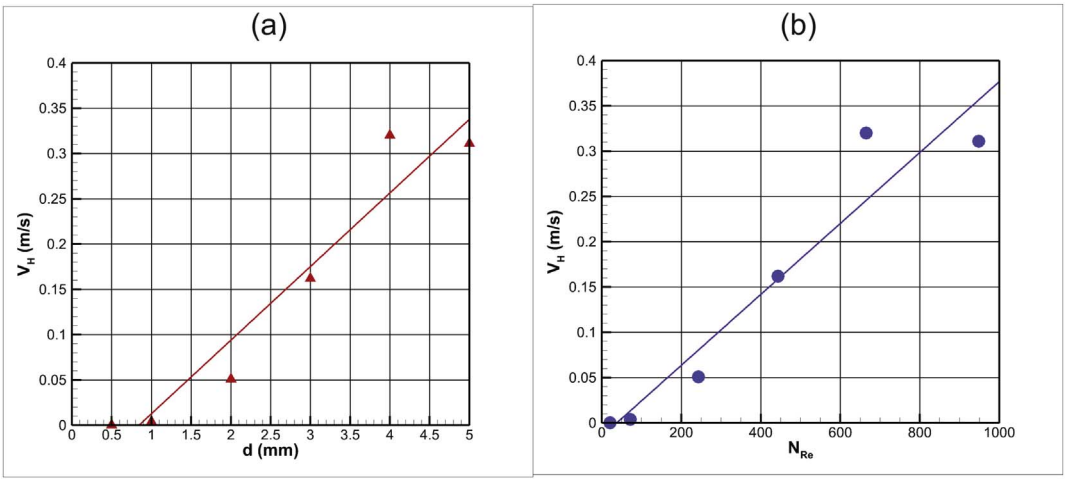

Fig. 13. The horizontal speed of conical graupel after they reach steady fall velocity as a function of (a) diameter, (b) Reynolds number.

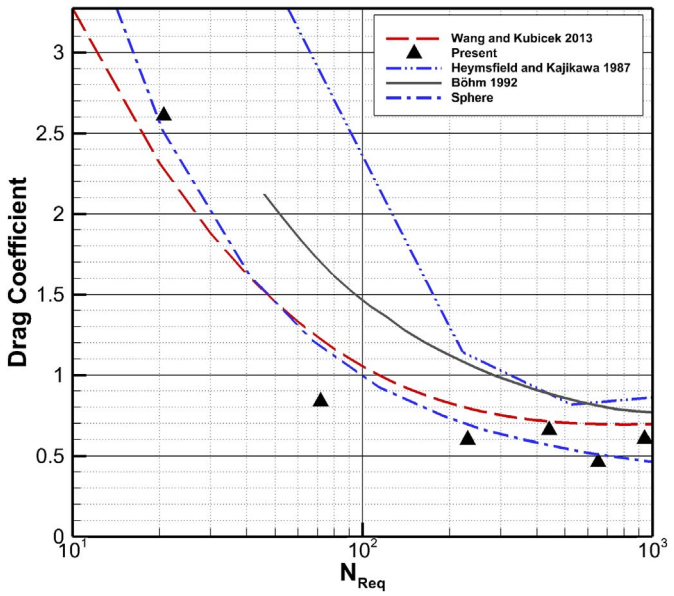

Fig. 14. Comparison of the drag coefficients as a function of Reynolds number calculated in the present study with some previous studies.

nonspherical shape. In Wang and Kubicek (2013) the graupel orientation is fixed and the shape effect is also fixed, causing deviations from the sphere drag. In the present case, the graupel is allowed to adjust its orientation in response to the nonspherical shape drag and thus partially compensate the shape factor. Hence it is reasonable to expect that the drag be closer to that of a sphere.

The drag coefficients of Heymsfield and Kajikawa (1987) and Böhm (1992) are higher than the present results possibly because of the difference in shape parameters. The graupel particles in the present study are all of the standard shape and aspect ratio, and surfaces are assumed to be smooth. The data used by Heymsfield and Kajikawa (1987) and Böhm (1992) were from observations of natural graupel whose shapes are not uniform and surfaces are not smooth. Roughness on the surface normally causes higher drag if all other factors remain the same. Hence it is reasonable to expect the drag coefficient to be higher.

From Fig. 14, it appears to be reasonable to use spherical drag coefficient to approximate the drag coefficient of a conical particle of the same Reynolds number. However, it is to be reminded that this approximation should be used only for drag calculations. As seen in the previous section, conical particles will perform significant horizontal translations which are probably not true for a spherical particle.

4. Summary and outlook

In the above sections, we reported our recent numerical simulation results of the free fall of conical graupel of idealized conical shape with smooth surface. We demonstrated that the computational fluid dynamical models can simulate the fall of conical graupel fairly realistically. All major motion modes – rotation, pendulum swing, sailing and tumbling – are successfully and realistically simulated. This shows that CFD packages can be used for calculations of hydrometeor motions in clouds. This is a much safer way to understand the hydrometeor dynamics than performing direct aircraft observations in clouds which can be dangerous and expensive. We have previously demonstrated that the motions of ice crystals (Cheng et al., 2015; Hashino et al., 2014, 2016) and hailstones (Cheng and Wang, 2013) can be successfully simulated. The present work fills an important gap for the understanding of large ice hydrometeors.

Natural graupel usually have various degrees of surface roughness which tend to cause higher drag on the conical body, as indicated by Fig. 14. We plan to perform simulations of the fall behavior of graupel with rough surface by simulating the roughness using the SMOSS technique described in Wang (1999).

It is also noted that this study is performed under the assumption that there is no turbulence imposed on the flow. Impact of externally imposed turbulence can be significant on the fall attitude and growth behavior of hydrometeors but it will require additional studies in the future.

One of the major gaps that still needs to be filled is the motions of snow aggregates (snowflakes). This knowledge is a necessity to understand the snow aggregation process which is a very large gap in cloud physics. We have already performed some tests using the same techniques as the present study and the preliminary results are encouraging. Hopefully we can report the full results in the near future.

Once the flow fields are obtained, it is possible to utilize these flow fields to perform ventilation coefficient and collision efficiency calculations for ice hydrometeors. We will also perform these studies in the near future.

Acknowledgments

This study is partially supported by the US NSF grant AGS-1633921 and research fund provided by the Academia Sinica, Taiwan. Any opinions, findings and conclusions or recommendations expressed in this material are those of the authors and do not necessarily reflect the views of the National Science Foundation (NSF). We thank Andrew Heymsfield and one anonymous reviewer for helpful comments that have led to improvements of this paper.

References

Böhm, H.P., 1992. A general hydrodynamic theory for mixed-phased microphysics. Part I: drag and fall speed of hydrometeors. Atmos. Res. 27, 253–274.

Cheng, K.Y., Wang, P.K., 2013. A numerical study of the flow fields around falling hails. Atmos. Res. 132-133, 253–263.

Cheng, K.Y., Wang, P.K., Hashino, T., 2015. A numerical study on dynamic snowflake. J. Atmos. Sci. 72, 3685–3698.

Chueh, C.C., Secanell, M., Bangerth, W., Djilali, N., 2010. Multi-level adaptive simulation of transient two-phase flow in heterogeneous porous media. Comput. Fluids 39, 1585–1596.

Chueh, C.C., Djilali, N., Bangerth, W., 2013. An h-adaptive operator splitting method for two-phase flow in 3D heterogeneous porous media. SIAM J. Sci. Comput. 35, B149–B175.

Chueh, C.C., Wang, P.K., Hashino, T., 2017. A preliminary numerical study on the time-varying fall attitudes and aerodynamics of freely falling conical graupel particles. Atmos. Res. 183, 58–72.

Cox, R.G., 1965. The steady motion of a particle of arbitrary shape at small Reynolds numbers. J. Fluid Mech. 23, 625–643.

Enzmann, F., Miedaner, M.M., Kersten, M., von Blohn, N., Diehl, K., Borrmann, S., Stampanoni, Ammann, M., Huthwelker, T., 2011. 3-D imaging and quantification of graupel porosity by synchrotron-based micro-tomography. Atmos. Meas. Tech. 4, 2225–2234.

Field, S.B., Klaus, M., Moore, M.G., Nori, F., 1997. Chaotic dynamics of falling disks. Nature 388, 252–254.

Goldstein, H., 1980. Classical Mechanics, 2nd ed. Addison-Wesley.

Hashino, T., Chiruta, M., Polzin, D., Kubicek, A., Wang, P.K., 2014. Numerical simulation of the flow fields around falling ice crystals with inclined orientation and the hydrodynamic torque. Atmos. Res. 150, 79–96.

Hashino, T., Cheng, K.-Y., Chueh, C.C., Wang, P.K., 2016. Numerical study of motion and stability of falling columnar crystals. J. Atmos. Sci. 73, 1923–1942.

Heymsfield, A.J., Kajikawa, M., 1987. An improved approach to calculating terminal velocities of plate-like crystals and graupel. J. Atmos. Sci. 44, 1088–1099.

Kajikawa, M., 1977. Observation of all attitude of conelike graupel particles. In: Memoirs of Fac. Education. 27. Akita University, pp. 78–85.

Kubicek, A., Wang, P.K., 2012. A numerical study of the flow fields around a typical conical graupel falling at various inclination angles. Atmos. Res. 118, 15–26.

Landau, L.D., Lifshitz, E.M., 1969. Mechanics, 2nd ed. Pergamon Press.

List, R., Schemenauer, R.S., 1971. Free-fall behavior of planar snow crystals, conical graupel and small hail. J. Atmos. Sci. 28, 110–115.

Locatelli, J.D., Hobbs, P.V., 1974. Fall speeds and masses of slid precipitation particles. J. Geophys. Res. 79, 2185–2197.

Pflaum, J.C., 1980. Hail formation via microphysical recycling. J. Atmos. Sci. 37, 160–173.

Pflaum, J.C., Pruppacher, H.R., 1979. A wind tunnel investigation of the growth of graupel initiated from frozen drops. J. Atmos. Sci. 36, 680–689.

Pflaum, J.C., Martin, J.J., Pruppacher, H.R., 1978. A wind tunnel investigation of the hydrodynamic behaviour of growing, freely falling graupel. Quart. J. R. Met. Soc. 104, 179–187.

Pruppacher, H.R., Klett, J.D., 1997. Microphysics of Clouds and Precipitation, 2nd ed. New York. (954 pp.).

Snyder, D.O., Koutsavdis, E.K., Anttonen, J.S.R., 2003. Transonic store separation using unstructured CFD with dynamic meshing. In: Technical Report AIAA-2003-3913. 33th AIAA Fluid Dynamics Conference and Exhibit. American Institute of Aeronautics and Astronautics.

Takahashi, T., 1978. Riming electrification as a charge generation mechanism in thunderstorms. J. Atmos. Sci. 35, 1536–1548.

Vincent, L., Shambaugh, W.S., Kanso, E., 2016. Holes stabilize freely falling coins. J. Fluid Mech. 801, 250–259.

Wang, P.K., 1982. Mathematical description of the shape of conical hydrometeors. J. Atmos. Sci. 39, 2615–2622.

Wang, P.K., 1983. On the definition of collision efficiency of atmospheric particles. J. Atmos. Sci. 40, 1051–1052.

Wang, P.K., 1999. Three-dimensional representations of hexagonal ice crystals and hailstone particles of elliptical cross sections. J. Atmos. Sci. 56, 1089–1093.

Wang, P.K., 2013. Physics and Dynamics of Clouds and Precipitation. Cambridge University Press, Cambridge (467 pp.).

Wang, P.K., Kubicek, A., 2013. Flow fields of graupel falling in air. Atmos. Res. 124, 158–169.

Williams, E.R., Zhang, R., 1996. Density of rime in laboratory simulations of thunderstorm microphysics and electrification. J. Geophys. Res.-Atmos. 101, 29715–29719.